Journal of Ocean Engineering and Technology 38(4), 174-186, August, 2024
https://doi.org/10.26748/KSOE.2024.055
pISSN 1225-0767
eISSN 2287-6715

Original Research Article

GCP Placement Methods for Improving the Accuracy of Shoreline Extraction in Coastal Video Monitoring

Changyul Lee[1], Kideok Do[2], Inho Kim[3], and Sungyeol Chang[4]

[1]Master Course, Department of Convergence study on the Ocean Science and Technology, Korea Maritime and Ocean University, Busan, Korea
[2]Associate Professor, Department of Ocean Engineering, Korea Maritime and Ocean University, Busan, Korea
[3]Professor, Department of Earth and Environmental Engineering, Kangwon National University, Samcheok, Korea
[4]Director, Haeyeon Engineering and Consultants Corporation, Gangneung, Korea

KEYWORDS: Coastal video monitoring, Direct linear transformation, Ground control points, Computer vision, Shoreline analysis, Coastal erosion

ABSTRACT: *In coastal video monitoring, the direct linear transform (DLT) method with ground control points (GCPs) is commonly used for geo-rectification. However, current practices often overlook the impact of GCP quantity, arrangement, and the geographical characteristics of beaches. To address this, we designed scenarios at Chuam Beach to evaluate how factors such as the distance from the camera to GCPs, the number of GCPs, and the height of each point affect the DLT method. Accuracy was assessed by calculating the root mean square error of the distance errors between the actual GCP coordinates and the image coordinates for each setting. This analysis aims to propose an optimal GCP placement method. Our results show that placing GCPs within 200 m of the camera ensures high accuracy with few points, whereas positioning them at strategic heights enhances shoreline extraction. However, since only fixed cameras were used in this study, factors like varying heights, orientations, and resolutions could not be considered. Based on data from a single location, we propose an optimal method for GCP placement that takes into account distance, number, and height using the DLT method.*

1. Introduction

In recent years, coastal erosion problems have arisen due to climate change and indiscriminate coastal development. Coastal erosion not only destroys ecosystems but also causes significant social and economic damage beyond the loss of sand, necessitating long-term monitoring and management (Ahmed et al., 2021; Rangel-Buitrago et al., 2018). This erosion is driven by complex processes such as rising sea levels, currents, waves, and wind (Dang et al., 2022). To assess coastal erosion and develop effective response strategies, various remote systems and methodologies for long-term coastline observation have been presented.

Global positioning system-real-time kinematic (GPS-RTK) measurement, a conventional monitoring method using walking or mobile equipment, presents low spatial resolution and requires considerable manpower and time for each measurement. Furthermore, it may result in position errors due to equipment shaking during kinematic surveying (Lee et al., 2013; Morton et al., 1993). To address these issues related to manpower, time, and spatial resolution, remote-monitoring technologies using drones, satellites, and video cameras have been developed.

Among remote-monitoring methods, aerial photography using drones offers high positional resolution in centimeters (cm). However, it incurs higher manpower costs compared to other methods and does not easily allow for continuous observations (Angnuureng et al., 2020; Luppichini et al., 2020; Zanutta et al., 2020). Satellite imagery can cover extensive areas but suffers from errors on the order of tens of meters (m) and low temporal resolution (Chen and Chang, 2009; Hagenaars et al., 2018; McAllister et al., 2022; Vos et al., 2019).

Coastal video systems, which use video cameras installed on beaches, offer real-time remote monitoring with an accuracy of several meters (m). Images obtained through coastal video monitoring have been used for analysis in 50 countries, including Australia, Italy, and the United Kingdom (Holman and Stanley, 2007; Kang et al., 2017; Stringari and Power, 2022; Valentini et al., 2017). Examples of their application include shoreline extraction, which uses average images

Received 13 June 2024, revised 17 July 2024, accepted 6 August 2024
Corresponding author Kideok Do: +82-51-410-5248, kddo@kmou.ac.kr

ⓒ 2024, The Korean Society of Ocean Engineers
This is an open access article distributed under the terms of the creative commons attribution non-commercial license (http://creativecommons.org/licenses/by-nc/4.0) which permits unrestricted non-commercial use, distribution, and reproduction in any medium, provided the original work is properly cited.

obtained by applying the arithmetic mean to images (Ribas et al., 2020); analysis of wave run-up using time stack images combining images captured over a certain duration (Simarro et al., 2015); identification of the effect of beach nourishment on shoreline changes (Santos et al., 2020); analysis of rip currents via sea-level monitoring (Surisetty et al., 2023); and monitoring of coastal waves using deep neural networks (Kim et al., 2020). In South Korea, Geosystem Research Corporation (GeoSR) has been used since 2003 to operate video monitoring systems at 40 locations, starting from Haeundae Beach in Haeundae-gu, Busan, Korea. It prepares average images using 60 to 180 images every 30 min starting from 07:00; subsequently, it extracts the shoreline and calculates the beach area based on the swash zone, which appears in dark white in the average images.

To quantitatively analyze beaches based on images, geo-rectification is required. Coastal video monitoring primarily uses the direct linear transformation (DLT) method for geo-rectification. This method involves a mathematical equation that expresses the relationship between image coordinates and ground coordinates with a linear function. Developed by Abdel-Aziz and Karara in 1971, it has been applied for coastal video monitoring since 1997, beginning in Holland and then expanding worldwide, including Korea (GeoSR). The DLT method can extract camera intrinsic and extrinsic parameters; additionally, it does not require initial value setting and repetitive calculations, unlike nonlinear equations. This method is primarily used for close-range photogrammetry and requires at least six ground control points (GCPs) to solve the 11 DLT parameters. Additionally, the results are sensitive to the number and placement of GCPs (Abdel-Aziz and Karara, 2015; Holland et al., 1997).

Most methods used to geo-rectify coastal videos utilize terrains outside of beaches that can be identified using a camera or based on coordinates observed directly within a beach as GCPs. Due to the characteristics of the DLT, the number and placement of GCPs significantly affect the accuracy of geo-rectification; however, related studies are limited. While some studies have investigated the appropriate placement of GCPs, they did not sufficiently consider the actual geographical characteristics of beaches, as they were conducted in digital virtual environments (Abdel-Aziz and Karara, 2015; Simarro et al., 2020).

In this study, we investigate methods for appropriately placing GCPs to improve the accuracy of geo-rectification, which is necessary when monitoring shorelines with video cameras installed on the coast. Data from a closed-circuit television (CCTV) installed at Chuam Beach in Donghae-si, Gangwon-do, Korea are used. GCPs are placed in various locations, and the accuracy of geo-rectification is analyzed. One CCTV unit has been operating at Chuam Beach since 2016, which is the target area of this study. The setting of GCPs and the accuracy of the geo-rectified image data are analyzed simultaneously with the image data via RTK-GPS observation. In this study, geo-rectification is performed using the DLT method as described above. To propose an optimal method for placing GCPs, we analyze the accuracy of geo-rectification based on the distance, number, and height of GCPs, as well as the external terrain of the beach, while considering the geographical characteristics of the beach.

2. Data Acquisition

2.1 Target Area

The target area of this study is a beach located in Chuam-dong, Donghae-si, Gangwon-do, Korea. Figure 1 shows the location and shape of the target area, as well as the installation location and field of view of the CCTV used for coastal video monitoring. The target area is a bow-shaped region connecting Chuam Beach and Jeungsan Beach, with an average beach width of approximately 63.4 m and a shoreline length of around 650 m. It is classified as a well-maintained and stable shoreline, according to the erosion-grade assessment from a coastal erosion survey conducted since 2010. A submerged breakwater (denoted in yellow in Fig. 1) was installed in front of the beach to address erosion issues potentially caused by the expanded breakwater at Donghae Port.

The video monitoring equipment used to observe shoreline changes in the target area was installed in the northern building of the Samcheok Sol Beach Hotel, located at the southern end of the beach,

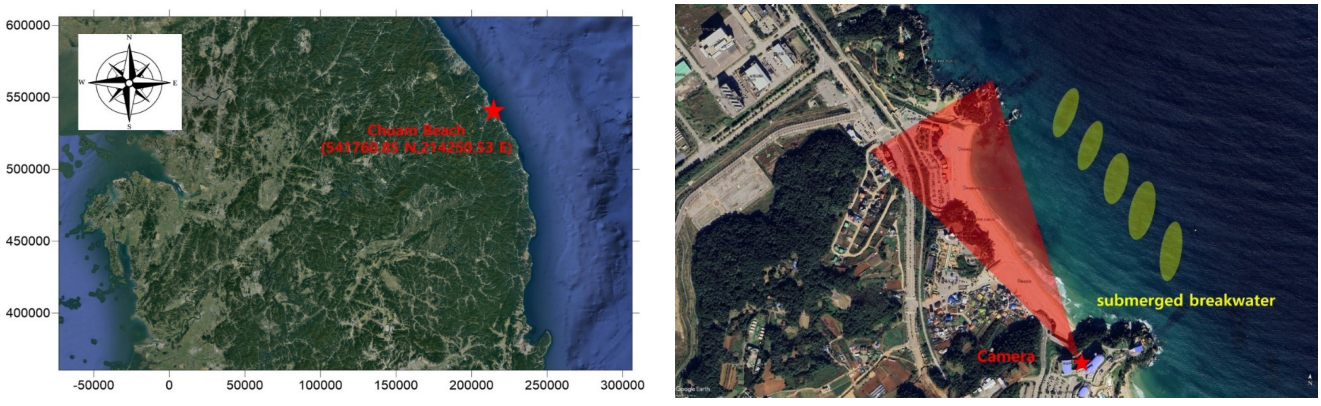

(a) (b)

Fig. 1 Map showing location and beach area of Chuam Beach: (a) Location of Chuam Beach (EPSG: 5187); (b) map of Chuam Beach showing the location of the camera and submerged breakwater.

(a) (b)

Fig. 2 (a) Camera installed at Chuam Beach; (b) sample image of Chuam Beach.

Table 1 Camera specifications

Model	Resolution	Frame rate	Focal length
IPC-PM2A-W	1920 × 1080	30 FPS	5.1–51 mm

as shown in Fig. 2(a). The installation position was approximately 60 m above sea level. Figure 2(b) shows the image (video) data acquired by the camera. As shown, the beach was monitored by minimizing obstacles such as bushes and beach trails. The model name, resolution, frame rate, and focal length of the installed camera are listed in Table 1. Due to the installation of the camera in a hazardous location, the extrinsic parameters, position, and orientation of the camera could not be precisely determined.

2.2 GCP Survey

In this study, geo-rectification was performed using the DLT method applied to the images (videos) acquired with the camera,

(a) (b)

Fig. 3 Distribution of ground control points viewed from Chuam Beach: (a) Google Earth; (b) camera image.

Table 2 Results of the GCP survey

	Date	Wave height	Sea level	Outside GCPs	Inside GCPs	Total GCPs
First Survey	2023. 10. 19. 11:00–12:45	0.5	16	7	28	35
Second Survey	2023. 12. 01. 12:13–13:00	1.4	4	0	68	68
Final GCPs				7	68	75

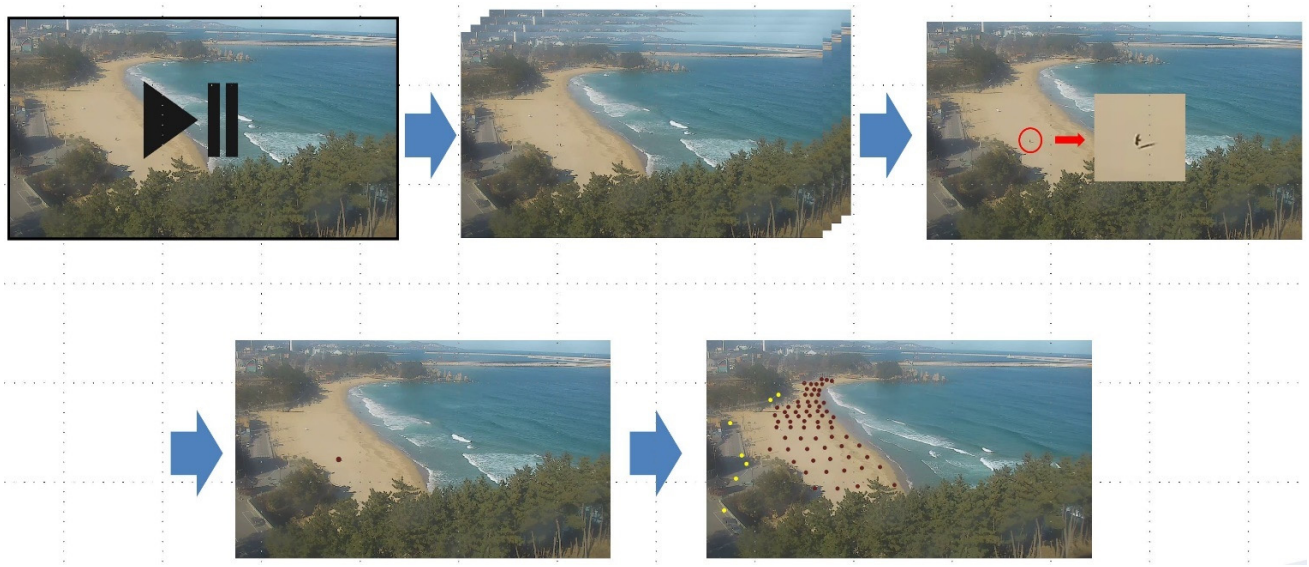

Fig. 4 Process of correlating image coordinates with GCP coordinates.

which involved setting the GCPs at appropriate locations. The GCPs were measured using GPS-RTK equipment. At each peak, stationary observations were conducted for 5 s, and the entire observation process was repeated twice. The equipment used was the "GPX3" model manufactured by Topcon Sokkia Positioning, which has horizontal and vertical position accuracies of approximately 3 and 5 mm, respectively. Figure 3 shows the positions of the GCPs acquired in this study, with GCPs inside and outside the beach denoted in red and yellow, respectively. As shown Fig. 3, 75 GCPs were acquired, including 68 and 7 GCPs inside and outside the beach, respectively. These GCPs were utilized for geo-rectification and accuracy analysis.

The first survey was conducted from 11:00 to 12:45 on October 19, 2023. During this survey, seven GCPs outside the beach (e.g., parking lines, speed bumps, and walking trails) and 28 GCPs inside the beach were observed. However, the GCP measurements were not regularly arranged based on distance and height, and the number of GCPs was insufficient. Therefore, a second survey was conducted from 12:13 to 13:00 on December 1, 2023. As shown in Fig. 3(a), GCPs were placed approximately 25 m apart along the beach, with a distance of about 10 m between the points, and 68 GCPs were observed. Table 2 shows details on the date, wave height, sea level, number of observed GCPs, and final observation results for each survey.

Fig. 4 shows the process of correlating image coordinates with GCP coordinates. This process was used to geo-rectify the spatial coordinate images (videos) acquired through the GCP survey. Image data were extracted at 1-s intervals from the video data during the observation period. The actual coordinates of the GCPs in the image were expressed by monitoring the positions of the GCPs as the acquired by the observer while moving during that time over time.

3. Image Data Processing

3.1 DLT Method

To quantify the information in image data, one must understand the photogrammetry transformation between three-dimensional actual coordinates and two-dimensional image coordinates. The DLT method, which was used for transforming actual coordinates (x, y, z) to the corresponding image coordinates (u, v), is described as follows: The transformation is performed based on the collinearity condition, which states that a point in actual space, the corresponding point on the image, and the projection center (x_c, y_c, z_c) must lie on the same straight line. Equation (1) shows the formula used to derive the DLT under the collinearity condition.

$$u-u_0 = -P_u\left[\frac{m_{11}(x-x_c)+m_{12}(y-y_c)+m_{13}(z-z_c)}{m_{31}(x-x_c)+m_{32}(y-y_c)+m_{33}(z-z_c)}\right] \quad (1)$$

$$v-v_0 = -P_v\left[\frac{m_{21}(x-x_c)+m_{22}(y-y_c)+m_{23}(z-z_c)}{m_{31}(x-x_c)+m_{32}(y-y_c)+m_{33}(z-z_c)}\right]$$

where

$$m_{11} = \cos\phi\cos\sigma+\sin\phi\cos\tau\sin\sigma,$$

$$m_{12} = -\sin\phi\cos\sigma+\cos\phi\cos\tau\cos\sigma,$$

$$m_{13} = -\sin\tau\cos\sigma$$

$$m_{21} = -\cos\phi\sin\sigma+\sin\phi\cos\tau\cos\sigma,$$

$$m_{22} = -\sin\phi\sin\sigma+\cos\phi\cos\tau\cos\sigma,$$

$$m_{23} = \sin\tau\cos\sigma,$$

$$m_{31} = \sin\phi\sin\tau,$$

$$m_{32} = \cos\phi\sin\tau,$$

$$m_{33} = -\cos\tau.$$

$P_u = \frac{f}{\lambda_u}$ and $P_v = \frac{f}{\lambda_v}$ represent the relationships between the horizontal/vertical scale factors (λ_u, λ_v) and the focal length (f), respectively. The elements ($m_{11}, m_{12}, \cdots, m_{33}$) are components of the rotation transformation matrix. Additionally, (ϕ, σ, τ) represent the three orientation angles of the camera, and (u_0, v_0) is the image center point. Collinearity equations, being nonlinear, require complex calculations. Therefore, these equations can be expressed as DLT equations by simplifying the six exterior orientation parameters (ϕ, σ, τ, x_c, y_c, z_c) and three interior orientation parameters (u_0, v_0, f) using DLT parameters (L_1–L_{11}), as shown in Eq. (2) (Abdel-Aziz and Karara, 2015; El-Ashmawy, 2018).

$$u = \frac{L_1X+L_2Y+L_3Z+L_4}{L_9X+L_{10}Y+L_{11}Z+1} \quad (2)$$

$$v = \frac{L_5X+L_6Y+L_7Z+L_8}{L_9X+L_{10}Y+L_{11}Z+1}$$

where

$$L = (x_cm_{31}+y_cm_{32}+z_cm_{33}),$$

$$L_1 = (u_0m_{31}+fm_{11})/(\lambda_uL),$$

$$L_2 = (u_0m_{32}+fm_{12})/(\lambda_uL),$$

$$L_3 = (u_0m_{33}+fm_{13})/(\lambda_uL),$$

$$L_4 = -(L_1x_c+L_2y_c+L_3z_c),$$

$$L_5 = m_{31}/L,$$

$$L_6 = m_{32}/L,$$

$$L_7 = m_{33}/L.$$

$$L_8 = (v_0m_{31}+fm_{21})/(\lambda_vL),$$

$$L_9 = (v_0m_{32}+fm_{22})/(\lambda_vL),$$

$$L_{10} = (v_0m_{33}+fm_{23})/(\lambda_vL),$$

$$L_{11} = -(L_8x_c+L_9y_c+L_{10}z_c),$$

At least six GCPs are required to perform geo-rectification using the DLT method. However, if initial estimates of the camera extrinsic and intrinsic parameters are provided, estimating the DLT parameter is possible using four or more GCPs (Holland et al., 1997). If the DLT parameters and image coordinates (u, v) are known, the image coordinates of the observed actual object can be directly calculated using the inverse of the equation given in Eq. (3).

$$\begin{bmatrix}[L_1-L_9u] & [L_1-L_9u] & [L_1-L_9u] \\ [L_1-L_9u] & [L_1-L_9u] & [L_1-L_9u]\end{bmatrix}\begin{bmatrix}x\\y\\z\end{bmatrix} = \begin{bmatrix}u-L_4\\v-L_8\end{bmatrix} \quad (3)$$

3.2 Geo-rectification

To perform geo-rectification, setting GCPs and establishing a correction process is crucial for estimating the camera's intrinsic and extrinsic parameters. Intrinsic parameters include the focal length (f_c), principal point (c_c), and radial and distortion coefficients (k_c), which correct for lens distortion and radiation effects. Extrinsic parameters include the camera position (x_c, y_c, z_c) and orientation angles (ϕ, σ, τ), which correct for the transformation relationship between the camera and actual coordinate system.

Generally, theses camera intrinsic and extrinsic parameters are estimated before installing the camera. However, since a pre-installed camera was used in this study, the intrinsic parameters were calculated by capturing checkerboard images on-site and using the camera calibration toolbox in MATLAB (Fetić et al., 2012). The extrinsic parameters were estimated using GPS-RTK equipment on-site. The acquired camera intrinsic and extrinsic parameters are shown in Table 3.

In this study, geo-rectification was performed using the Quantitative Coastal Imaging Toolbox (QCIT) developed by the Coastal Imaging Research Network (CIRN). This toolbox is designed for generating coastal imaging analysis data using unmanned aerial vehicles or single/multiple cameras. It can perform geo-rectification by extracting images from videos. The CIRN QCIT processes data in the following order: preprocessing (extracting images from video files), camera calibration (solving camera extrinsic parameters), projection-domain definition, image stabilization, and corrected-data processing (Bruder and Brodie, 2020). The resulting orthoimages were set to a resolution of 1 m per pixel, with a size of 600 × 600 pixels.

Table 3 Camera intrinsic and extrinsic parameters

Intrinsic parameters	
component of principal point (u_0, v_0)	945.5359, 532.9340
components of focal lengths (f_x, f_y)	2135.6442, 2156.1282
Radial distortion coefficient (d_1, d_2, d_3)	-0.2153, 0.0586, 0
Tangential distortion coefficient (t_1, t_2)	0, 0
External parameters	
camera position (x, y, z)	214512.4245, 541473.9769, 59.7033
azimuth, tilt and swing (ϕ, σ, τ)	-0.4719, 1.3291, 0.0116

Additionally, the CIRN QCIT applies the elevation value entered by the user to orthoimages across the entire XY grid. Higher accuracy is achieved when the elevation of the actual coordinates in the orthoimage closely matches the input elevation. Since the purpose of this study is to extract shorelines, tidal data from the Donghae Port Tidal Observatory in Donghae Port, Gangwon-do, Korea, were utilized to ensure the highest accuracy for shoreline positions. The input elevation was set to 0.9 m, corresponding to the sea-level height at the time of imaging.

4. Research Method and Results

4.1 Design and Research Method for GCP Placement

In this study, the accuracy between the actual GCP coordinates and the GCP coordinates obtained via the DLT method was analyzed. The goal was to identify GCP setting factors that improve image resolution during geographic calibration, ensuring accurate alignment between CCTV data and actual coordinates, and to propose optimal deployment methods. GCP placements were designed considering the distance from the camera, the number of GCPs, and their height, as summarized in Table 4. The effect of these elements on geo-rectification accuracy was subsequently analyzed. Figure 5 shows the distribution of GCPs set for each scenarios, with point colors indicating the elevations assigned to the GCPs.

D1 to D4 in Table 4 represent the scenarios for analyzing the effect of the distance from the camera on GCP settings and geo-rectification accuracy. In high-oblique imaging, as used in coastal video monitoring, the image scale is not uniform compared to vertical imaging. In particular, as the distance of a point from the camera increases, the spatial resolution of a pixel decreases, which rapidly degrades the ability to identify the target. Therefore, we assumed that the distance from the camera would significantly affect the accuracy of geo-rectification. To evaluate this, distances of approximately 200 m (D1), 300 m (D2), 400 m (D3), and 700 m (D4) from the camera were used. Each scenario maintained a consistent distribution by placing two or three GCPs along each baseline, as shown in Fig. 5.

Next, six scenarios were designed to analyze the effect of the number of GCPs on geo-rectification accuracy, using 6, 9, and 15 GCPs. In these scenarios, GCPs were placed within 200 m for N1, N2, and N3, and between 200 and 300 m for N4, N5, and N6. For the DLT method used in this study, increasing the number of GCPs reduces error through the least-squares method, as redundant information contributes to the overdetermined system, as detailed in Section 3. This generally improves the accuracy of the orthoimage as the number of GCPs set during the geo-rectification process increases, but the scenarios were designed with the expectation that beyond a certain number, the improvement in accuracy would be limited.

The GCPs setting scenarios H1 to H3 were designed to analyze the effect of GCP elevation on the accuracy of geo-rectified images. According to the theoretical formula (Eq. (2)) of the DLT method described in chapter 3, the results of geo-rectified image can vary depending on the elevation (z) the GCPs used. To achieve highly accurate geo-rectification, it is anticipated that GCPs need to be evenly distributed entire elevation range of the beach. Thus, these scenarios included six GCPs within 200 m, as shown in Fig. 5, with three different height distributions: concentrated at the bottom (H1) or top (H2) of the beach for H1 and H2, and evenly distributed across the beach for H3.

Table 4 GCP setting scenarios

	Number of GCPs	Distance of GCPs (m)	Height of GCPs (m)
(D1)	9	227	[0.28–3.44]
(D2)	18	313	[0.36–3.00]
(D3)	27	397	[0.87–3.00]
(D4)	37	684	[0.95–2.90]
(N1)	6	227	[0.28–3.44]
(N2)	9	227	[0.28–3.44]
(N3)	15	227	[0.28–3.44]
(N4)	6	227–313	[0.95–3.00]
(N5)	9	227–313	[0.95–3.00]
(N6)	15	227–313	[0.95–3.00]
(H1)	6	227	[1.74–3.44]
(H2)	6	227	[0.95–1.56]
(H3)	6	227	[0.95–3.44]
(Outside of beach)	5	313	[3.49–12.06]

The outside-of-beach scenario, commonly used in previous studies, involves using GCPs from fixed terrains outside the beach. This method is favored because fixed terrains are easy to identify and can be consistently used even if the camera orientation changes. However, since coastal video monitoring typically targets the beach, fixed points outside the beach—being distant from the camera and at higher elevations—may introduce errors near the shoreline. To address this, we created a scenario with five GCPs, including parking lines, speed bumps, and coastal road lanes located outside the beach.

In this study, geo-rectification was performed using the CIRN QCIT software, as described in Section 3, across the 12 scenarios outlined in Table 4. The accuracy of the geo-rectified images was subsequently analyzed. Figure 6 shows images with GCP coordinates (a) before and (b) after geo-rectification. Following the application of the DLT method, the coordinate-system information of the images was extracted. The accuracy of the geo-rectified images was quantified by calculating the along-shore and cross-shore distance errors, as well as the total distance error, based on the actual GCP coordinates acquired from the images. These errors were measured using the root-mean-square error (RMSE) metric.

4.2 Geo-rectification Result Analysis: Distance and Quantity

Table 5 shows the RMSE of each orthoimage generated under scenarios D1 to D4 and N1 to N3, which were designed based on the distance from the camera and the number of GCPs. First, under scenarios

D1 to D4, the RMSEs of the total distance were calculated as follows: D1 = 7.07 m, D2 = 7.42 m, D3 = 9.20 m, and D4 = 11.23 m. Notably, the RMSE increased significantly after 300 m, with increments of 0.35, 1.78, and 2.03 m as the distance increased. For scenarios N1 to N3, the RMSEs were : N1 = 7.02 m, N2 = 7.07 m, N3 =7.01 m, N4 = 8.73 m, N5 = 9.21 m, and N6 = 9.90 m. Contrary to the expectation that the accuracy

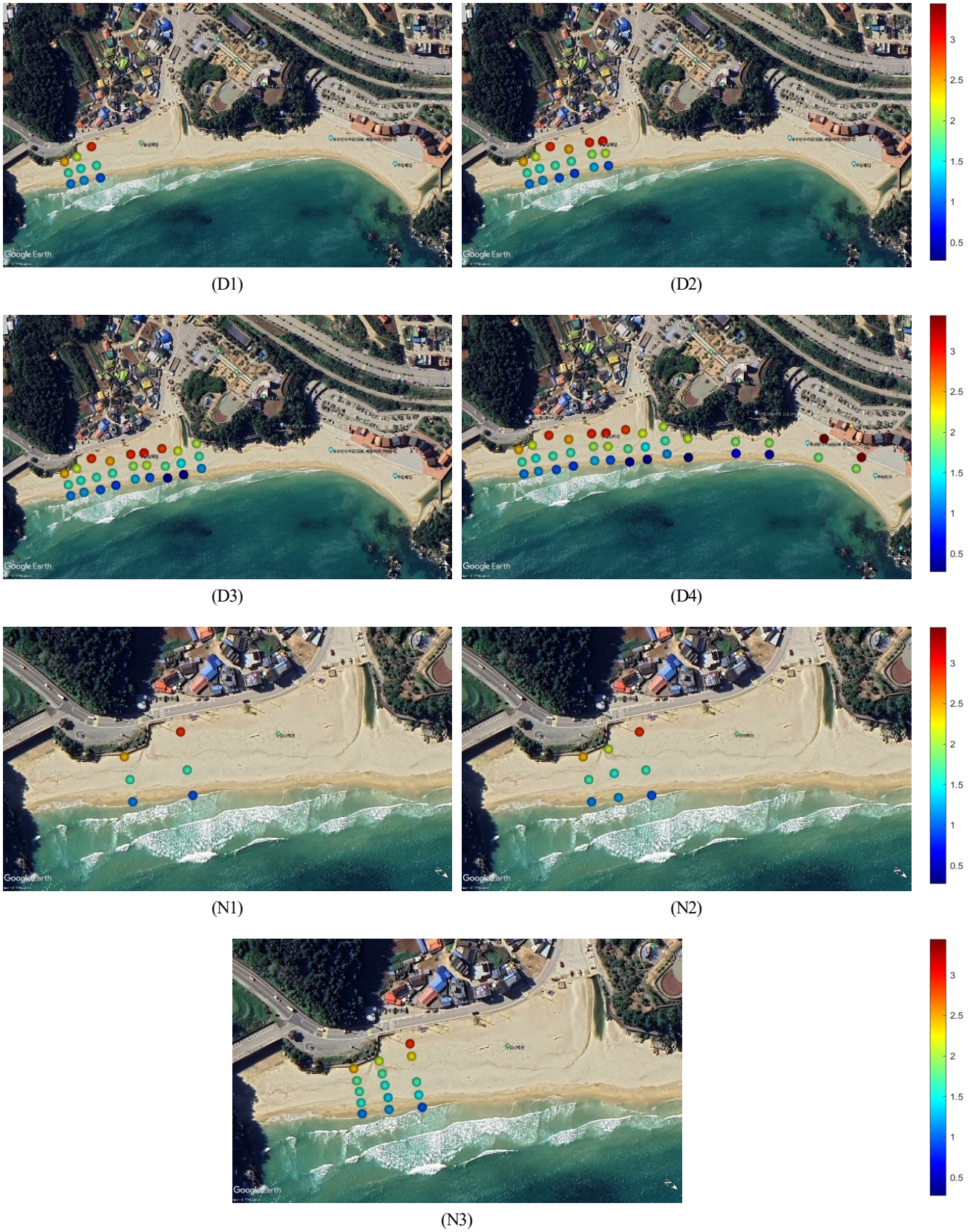

Fig. 5 Distribution of GCPs (points) and their elevations.

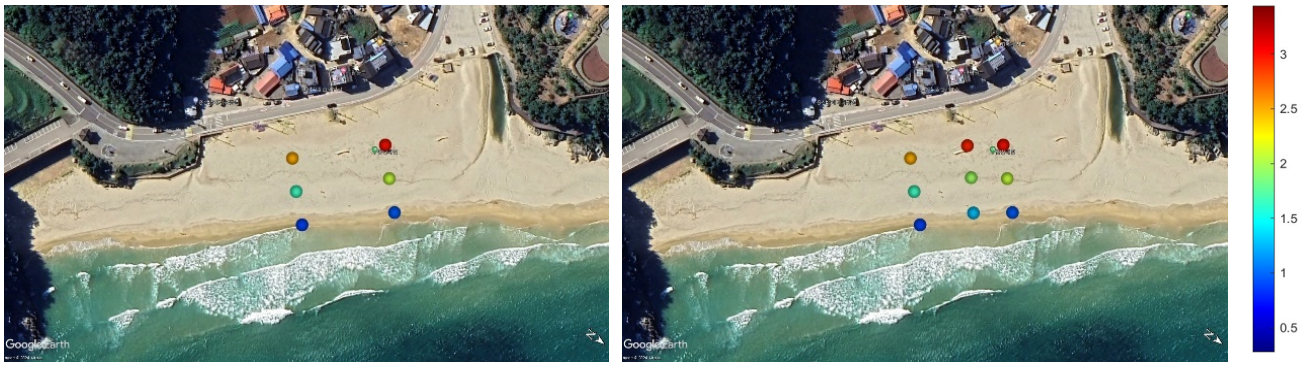

(N4) (N5)

(N6)

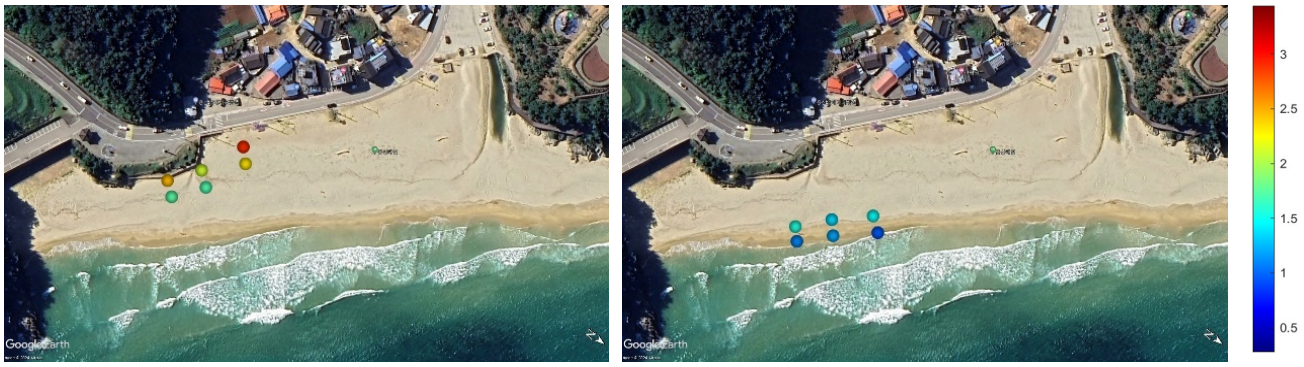

(H1) (H2)

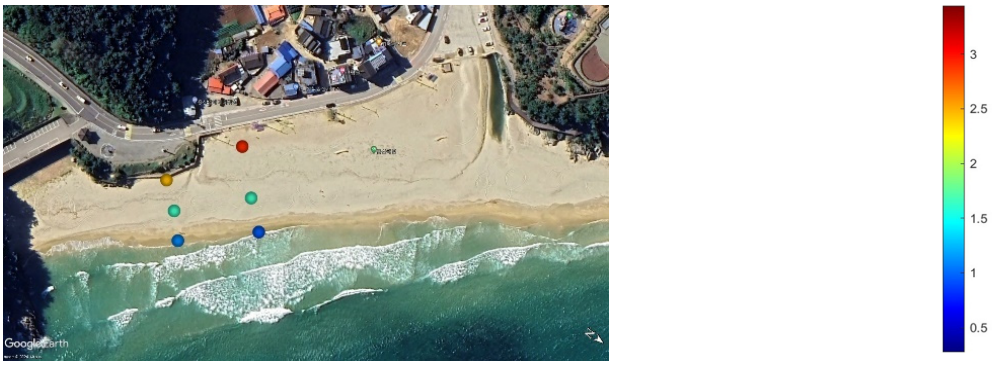

(H3)

Fig. 5 Distribution of GCPs (points) and their elevations (Continuation).

improvement would be limited with increasing number of GCPs, the RMSE rather increased for distances between 200 and 300 m. However, within 200 m, the RMSE did not vary significantly, with a difference of 0.05 m or less. An analysis of the RMSE values for along- and cross-shore distances from D1 to N6 reveals that they increased proportionally with the total-distance RMSE.

(a)

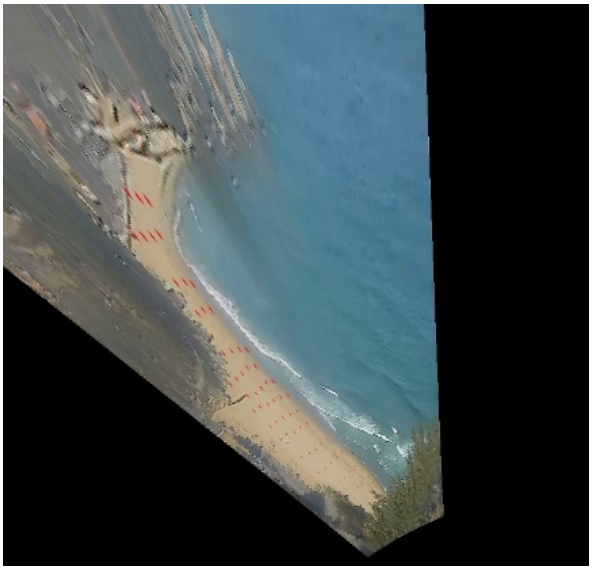

(b)

Fig. 6 Chuam images: (a) Marked Chuam image with GCP coordinates; (b) geo-rectified Chuam image.

Table 5 Accuracy of coordinate transformation

	$(RMSE)_{xy}$	$(RMSE)_x$	$(RMSE)_y$
(D1)	7.07	5.76	4.04
(D2)	7.42	6.10	4.15
(D3)	9.20	7.48	5.30
(D4)	11.23	9.16	6.43
(N1)	7.02	5.70	4.02
(N2)	7.07	5.76	4.04
(N3)	7.01	5.67	4.01
(N4)	8.73	7.01	5.10
(N5)	9.21	7.45	5.32
(N6)	9.90	8.14	5.57

The analysis of scenarios D1 to D4 shows that the total RMSE increases with distance beyond 200 m, even when the number of GCPs is increased. This increase in RMSE can be attributed to the decrease in pixel spatial resolution with greater distance, which is characteristic of high-oblique imaging.

For scenarios N1 to N3, the difference in RMSE was 0.05 m or less, indicating that increasing the number of GCPs does not significantly improve the positional accuracy of geo-rectified images with a resolution of 1 m per pixel. However, the results from scenarios N4 to N6 show that error increase with the number of GCPs once a certain distance threshold is exceeded. This suggests that high positional accuracy can be achieved with fewer GCPs if they are within 200 meters of the camera. Conversely, adding more GCPs beyond this

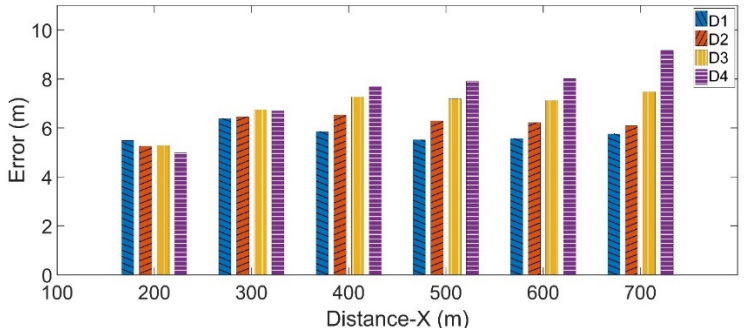

(a)

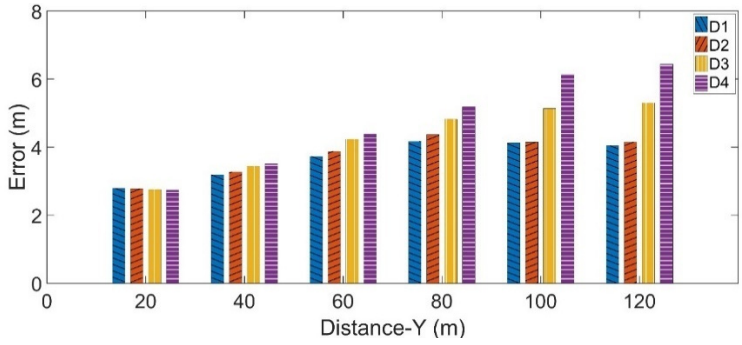

(b)

Fig. 7 Error with respect to (a) along-shore distance and (b) cross-shore distance.

distance may introduce significant errors. In conclusion, choosing the appropriate distance for GCP placement is more critical than the sheer number of GCPs to achieve high positional accuracy in orthoimages. When it is challenging to use GCPs within the optimal distance, it is advisable to use the minimum number of GCPs necessary for geo-rectification.

This study analyzed the impact of distance on error for coastal video monitoring aimed at observing extensive beach areas along the shoreline. Figure 7 illustrates the error based on along- and cross-shore distances from the camera for scenarios D1 to D4. The results show that the error that occurs with distance also increases as the RMSE of the total distance increases, highlighting the need for high positional resolution when monitoring long shorelines, such as Chuam Beach, with a single camera.

4.3 Geo-rectification Result Analysis: Height and Terrain Outside of Beach

Table 6 shows the RMSE of each orthoimage generated under the scenarios H1 to H3, which were designed based on the height of the GCPs, as well as the outside-of-beach scenario, which involved terrains outside the beach. For the height-based scenarios, the RMSE values were calculated as follows: H1 = 9.27 m, H2 = 7.16 m, and H3 = 7.02 m. Among these, H3, which evenly distributed GCPs across the beach width, achieved the highest positional resolution, with an RMSE of 7.02 m., which concentrated GCPs only at the top of the beach, indicated an RMSE of 7.16 m, which was 0.14 m higher than that indicated by H3. H1, which concentrated GCPs at the bottom of the beach, showed the lowest accuracy, with an RMSE of 9.27 m, which was 2.11 m higher than H2. The RMSE for the orthoimages using terrains outside the beach was 9.58 m, which is 1.65 m lower than D4, the scenario with the highest RMSE in the experiment, but only 0.4 m or less different from D3 and H1. Notably, this outside-of-beach scenario had the lowest accuracy in the study.

Table 6 Accuracy of coordinate transformation

	$(RMSE)_{xy}$	$(RMSE)_x$	$(RMSE)_y$
(H1)	9.27	7.26	5.64
(H2)	7.16	5.67	4.2
(H3)	7.02	5.70	4.02
(Outside of beach)	9.58	7.72	5.56

When comparing the RMSEs of the along- and cross-shore distances, RMSE of H2 for the total distance was 0.14 m higher than H3. However, the RMSE of H3 for the along-shore distance was 0.03 m higher, while H2 showed a significant difference of 1.8 m for the cross-shore distance. For H1 and the outside-of-beach scenario, the RMSE of the along-shore distance was 0.46 m higher in the outside-of-beach scenario, whereas the cross-shore distance RMSE was 0.08 m higher in H1.

Fig. 8 shows the positional error at various height intervals of GCPs in the orthoimages of H1, H2, and H3. At points with a height of 0 to 1 meter on the beach, where GCPs had a relatively low elevation, H1, which used GCPs at lower heights, demonstrated high accuracy. However, as the height increased beyond 1 m, the error also increased, with H2 and H3, which used GCPs at higher elevations, exhibiting higher accuracy. This shows that appropriate placement, such as in H3,

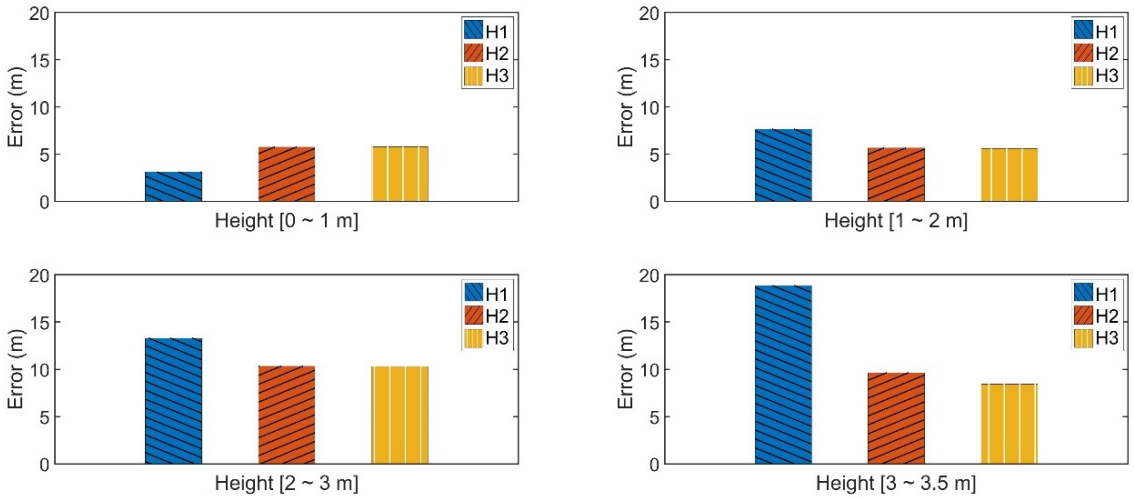

Fig. 8 Error at various height intervals of GCPs.

is required to achieve a high position resolution for the entire beach. In this study, however, performing geo-rectification using GCPs close to the shoreline may present results that are more suitable for observing changes in the shoreline position, beach width, and beach area, which is the main purpose of coastal video monitoring.

5. Discussion

In this study, we investigated the effects of the number and placement of GCPs on the high positional resolution of orthoimages, specially focusing on improving the position resolution for coastal monitoring systems. We acquired 68 and 7 GCPs inside and outside Chuam Beach, respectively. These GCPs were used to design scenarios considering factors such as distance from the camera to the GCPs, the number of GCPs, the height of GCPs, and the use of terrains outside the beach. Orthoimages were generated using the DLT method, and their accuracy was evaluated by measuring distance errors between the geo-rectified image coordinates and actual GCP coordinates, as well as by calculating the RMSE.

First, images were geo-rectified using GCPs placed at distances of 200, 300, 400, and 700 m from the camera. The RMSE for total distance errors were found to be 7.07, 7.42, 9.20, and 11.23 m, respectively. The highest accuracy was obtained with GCPs within 200 m. Error analysis based on the along- and cross-shore distances further demonstrated that maintaining GCPs within 200 meters consistently yielded high accuracy, even at longer distances.

Next, images were geo-rectified using 6, 9, and 15 GCPs within 200 m and between 200 and 300 m, respectively, to examine the positional resolution with varying numbers of GCPs. The accuracy improves with the number of GCPs, but the rise was expected to be limited, but the RMSE for orthogonal images within 200 m was 7.02, 7.07, and 7.01 m, showing a minimum difference of less than 0.05. Conversely, the RMSE for GCPs placed between 200 and 300 meters was 8.93, 9.21, and 9.90 meters, showing an increase in error. This study confirms that high accuracy can be achieved even with a smaller number of GCPs, provided they are within an appropriate distance. It also demonstrates that accuracy may decrease when GCPs are placed beyond a certain distance. Thus, placing GCPs within an optimal distance is recommended, while using the minimum number necessary when positioning GCPs at greater distances.

To analyze the effect of GCP height, orthoimages were generated under three scenarios: GCPs concentrated at the bottom, the top of the beach, or evenly distributed across the beach. The RMSEs were calculated as 9.27, 7.16, and 7.02 m respectively. The scenario with evenly distributed GCPs across the beach showed the lowest error. However, for calculating the shoreline position and the width and area of the beach, using GCPs close to the shoreline is more suitable based on error analysis.

Finally, the position resolution of orthoimages using GCPs from outside-the-beach terrains was analyzed. Orthoimages were generated using five terrains, e.g., parking lines, speed bumps, and lanes, as GCPs. The RMSE for these orthoimages was 9.58 m. Given the lowest accuracy observed among all scenarios, using only outside-the-beach terrains as GCPs is unsuitable for coastal video monitoring at Chuam Beach.

6. Conclusion

In this study, we demonstrated that placing a few GCPs within 200 m of a camera achieved high positional resolution even from a long distance along the shoreline of Chuam Beach. However, for shoreline extraction, which is the aim of this study, using GCPs close to the shoreline is recommended. Additionally, using terrains outside the beach as GCPs proved unsuitable because these GCPs were distant from the camera and excessively high above the beach.

During the generation of orthoimages, the optimal placement of GCPs may vary depending on the camera's resolution, position, and orientation. In this study, however, only a single camera was used for Chuam Beach, and the camera height and orientation were fixed. Therefore, variations in camera resolutions, heights, and orientations

could not be considered. Future research should aim to develop an optimal geo-rectification method by expanding coastal monitoring to various beaches.

Orthoimages in this study were generated using the DLT method with data from a single point, and an optimal GCP placement method was proposed by considering the distance, number, and height of GCPs. The results showed that GCPs should be placed within an appropriate distance from the camera to generate high accuracy orthoimages. High accuracy can be secured without numerous GCPs if the GCPs are placed within this appropriate distance. If GCPs are placed beyond this distance, however, the minimum number of GCPs required should be used. For accurate shoreline extraction, GCPs with low elevation near the shoreline are recommended. If terrains outside the beach are used as GCPs, their placement must consider both the appropriate distance and the height difference from the target.

Conflict of Interest

Kideok Do serves as the journal-publication committee member of the Journal of Ocean Engineering and Technology; however, he is not involved with the decision to publish this article. The authors declare no potential conflict of interest relevant to this article.

Funding

This study was supported by the National Research Foundation of Korea, which is grant funded by the Korea government (RS-2023-00256687), and through the project titled, “Cyclic Adaptive Coastal Erosion Management Technology Development” funded by the Ministry of Oceans and Fisheries of Korea.

References

Abdel-Aziz, Y. I., & Karara, H. M. (2015). Direct linear transformation from comparator coordinates into object space coordinates in close-range photogrammetry. *Photogrammetric Engineering & Remote Sensing, 81*(2), 103−107. https://doi.org/10.14358/PERS.81.2.103

Ahmed, N., Howlader, N., Hoque, M. A. A., & Pradhan, B. (2021). Coastal erosion vulnerability assessment along the eastern coast of Bangladesh using geospatial techniques. *Ocean and Coastal Management, 199*, 105408. https://doi.org/10.1016/j.ocecoaman.2020.105408

Angnuureng, D. B., Jayson-Quashigah, P. N., Almar, R., Stieglitz, T. C., Anthony, E. J., Aheto, D. W., & Addo, K. A. (2020). Application of shore-based video and unmanned aerial vehicles (Drones): Complementary tools for beach studies. *Remote Sensing, 12*(3), 394. https://doi.org/10.3390/rs12030394

Bruder, B. L., & Brodie, K. L. (2020). CIRN quantitative coastal imaging toolbox. *SoftwareX, 12*, 100582. https://doi.org/10.1016/j.softx.2020.100582

Chen, W. W., & Chang, H. K. (2009). Estimation of shoreline position and change from satellite images considering tidal variation. *Estuarine, Coastal and Shelf Science, 84(*1), 54−60. https://doi.org/10.1016/J.ECSS.2009.06.002

Dang, K. B., Dang, V. B., Ngo, V. L., Vu, K. C., Nguyen, H., Nguyen, D. A., Nguyen, T. D. L., Pham, T. P. N., Giang, T. L., Nguyen, H. D., & Hieu Do, T. (2022). Application of deep learning models to detect coastlines and shorelines. *Journal of Environmental Management, 320*, 115732. https://doi.org/10.1016/j.jenvman.2022.115732

El-Ashmawy, K. L. A. (2018). Using direct linear transformation (DLT) method for aerial photogrammetry applications. *Geodesy and Cartography, 44*(3), 71−79. https://doi.org/10.3846/gac.2018.1629

Fetić, A., Jurić, D., & Osmanković, D. (2012). The procedure of a camera calibration using Camera Calibration Toolbox for MATLAB. In *2012 Proceedings of the 35th International Convention MIPRO* (pp. 1752−1757). IEEE.

Hagenaars, G., de Vries, S., Luijendijk, A. P., de Boer, W. P., & Reniers, A. J. H. M. (2018). On the accuracy of automated shoreline detection derived from satellite imagery: A case study of the sand motor mega-scale nourishment. *Coastal Engineering, 133*, 113−125. https://doi.org/10.1016/j.coastaleng.2017.12.011

Holland, K. T., Holman, R. A., Lippmann, T. C., Stanley, J., & Plant, N. (1997). Practical Use of Video Imagery in Nearshore Oceanographic Field Studies. *IEEE Journal of Oceanic Engineering, 22*(1), 81−92. https://doi.org/10.1109/48.557542

Holman, R. A., & Stanley, J. (2007). The history and technical capabilities of Argus. *Coastal Engineering, 54*(6−7), 477−491. https://doi.org/10.1016/j.coastaleng.2007.01.003

Kang, T.-S., Kim, J.-B., Kim, G.-Y., Kim, J.-K., & Hwang, C.-S. (2017). Variation characteristics of Haeundae Beach using video image. *Journal of Ocean Engineering and Technology, 31*(1), 60−68. https://doi.org/10.5574/KSOE.2017.31.1.060

Kim, J., Kim, J., Kim, T., Huh, D., & Caires, S. (2020). Wave-tracking in the surf zone using coastal video imagery with deep neural networks. *Atmosphere, 11*(3), 304. https://doi.org/10.3390/atmos11030304

Lee, J.-M., Park, J.-Y., & Choi, J.-Y. (2013). Evaluation of sub-aerial topographic surveying techniques using total station and RTK-GPS for applications in macrotidal sand beach environment. *Journal of Coastal Research, 65*(sp1), 535−540. https://doi.org/10.2112/si65-091.1

Luppichini, M., Bini, M., Paterni, M., Berton, A., & Merlino, S. (2020). A new beach topography-based method for shoreline identification. *Water*, *12*(11), 3110. https://doi.org/10.3390/w12113110

McAllister, E., Payo, A., Novellino, A., Dolphin, T., & Medina-Lopez, E. (2022). Multispectral satellite imagery and machine learning for the extraction of shoreline indicators. *Coastal Engineering, 174*, 104102. https://doi.org/10.1016/J.COASTALENG.2022.104102

Morton, R. A., Leach, M. P., Paine, J. G., & Cardoza, M. A. (1993). Monitoring beach changes using GPS surveying techniques. *Journal of Coastal Research,* 9(3), 702−720.

Rangel-Buitrago, N., Williams, A. T., & Anfuso, G. (2018). Hard protection structures as a principal coastal erosion management strategy along the Caribbean coast of Colombia. A chronicle of pitfalls. *Ocean & Coastal Management, 156*, 58−75. https://doi.org/10.1016/j.ocecoaman.2017.04.006

Ribas, F., Simarro, G., Arriaga, J., & Luque, P. (2020). Automatic shoreline detection from video images by combining information from different methods. *Remote Sensing, 12*(22), 3717. https://doi.org/10.3390/rs12223717

Santos, C. J., Andriolo, U., & Ferreira, J. C. (2020). Shoreline response to a sandy nourishment in a wave-dominated coast using video monitoring. *Water, 12*(6), 1632. https://doi.org/10.3390/W12061632

Simarro, G., Bryan, K. R., Guedes, R. M. C., Sancho, A., Guillen, J., & Coco, G. (2015). On the use of variance images for runup and shoreline detection. *Coastal Engineering, 99*, 136−147. https://doi.org/10.1016/j.coastaleng.2015.03.002

Simarro, G., Calvete, D., Souto, P., & Guillén, J. (2020). Camera calibration for coastal monitoring using available snapshot images. *Remote Sensing, 12*(11), 1840. https://doi.org/10.3390/rs12111840

Stringari, C. E., & Power, H. (2022). Picoastal: A low-cost coastal video monitoring system. *SoftwareX, 18*, 101073. https://doi.org/10.1016/j.softx.2022.101073

Surisetty, V. V. A. K., Venkateswarlu, C., Ramesh, M., Gireesh, B., Naidu, C. V., Sheela Nair, L., & Sharma, R. (2023). Practical use of smartphone cameras in rip current monitoring studies. *Ocean & Coastal Management, 243*, 106776. https://doi.org/10.1016/j.ocecoaman.2023.106776

Valentini, N., Saponieri, A., & Damiani, L. (2017). A new video monitoring system in support of coastal zone management at Apulia region, Italy. *Ocean & Coastal Management, 142*, 122−135. https://doi.org/10.1016/j.ocecoaman.2017.03.032

Vos, K., Harley, M. D., Splinter, K. D., Simmons, J. A., & Turner, I. L. (2019). Sub-annual to multi-decadal shoreline variability from publicly available satellite imagery. *Coastal Engineering, 150*, 160−174. https://doi.org/10.1016/J.COASTALENG.2019.04.004

Zanutta, A., Lambertini, A., & Vittuari, L. (2020). UAV photogrammetry and ground surveys as a mapping tool for quickly monitoring shoreline and beach changes. *Journal of Marine Science and Engineering, 8*(1), 52. https://doi.org/10.3390/JMSE8010052

Author ORCIDs

Author name	ORCID
Lee, Changyul	0009-0004-6206-2829
Do, Kideok	0000-0001-7364-8375
Kim, Inho	0000-0003-3466-588X
Chang, Sungyeol	0000-0003-4641-4383